Published in final edited form as:
Nat Med. 2015 December ; 21(12): 1497–1501. doi:10.1038/nm.3994.

Microbiota depletion promotes browning of white adipose tissue and reduces obesity

Nicolas Suárez-Zamorano[#1,2], **Salvatore Fabbiano**[#1,2], **Claire Chevalier**[1,2], **Ozren Stojanović**[1,2], **Didier J. Colin**[3], **Ana Stevanović**[1,2], **Christelle Veyrat-Durebex**[1,2], **Valentina Tarallo**[1,2], **Dorothée Rigo**[1,2], **Stéphane Germain**[3], **Miroslava Ilievska**[4], **Xavier Montet**[5], **Yann Seimbille**[6], **Siegfried Hapfelmeier**[7], and **Mirko Trajkovski**[1,2,8,†]

[1]University of Geneva, Faculty of Medicine, Department of Cell Physiology and Metabolism, Centre Médical Universitaire (CMU), Geneva, Switzerland [2]University of Geneva, Diabetes Centre, Faculty of Medicine, Geneva, Switzerland [3]University Hospital of Geneva, Centre for BioMedical Imaging (CIBM), Geneva, Switzerland [4]Alkaloid AD Skopje, Skopje, Republic of Macedonia [5]University Hospital of Geneva, Division of radiology, Geneva, Switzerland [6]University Hospital of Geneva, Cyclotron unit, Division of Nuclear Medicine, Geneva, Switzerland [7]University of Bern, Institute for Infectious Diseases, Bern, Switzerland [8]University College London (UCL), Division of Biosciences, Institute of Structural and Molecular Biology, London, UK

[#] These authors contributed equally to this work.

Abstract

Brown adipose tissue (BAT) promotes a lean and healthy phenotype and improves insulin sensitivity[1]. In response to cold or exercise brown fat cells also emerge in the white adipose tissue (named beige cells), a process known as browning[2,3,4]. Here, we show that the development of functional beige fat is promoted by microbiota depletion either by antibiotic treatment or in germ-free mice within the inguinal subcutaneous and perigonadal visceral adipose tissues (ingSAT and pgVAT, respectively). This leads to improved glucose tolerance, insulin sensitivity and decreased white fat and adipocyte size in lean mice and obese leptin-deficient (ob/ob) and high fat diet (HFD)-fed mice. These metabolic improvements are mediated by eosinophil infiltration and enhanced type 2 cytokine signaling and M2 macrophage polarization in the subcutaneous white fat depots of microbiota-depleted animals. The metabolic phenotype and the browning of the subcutaneous fat are impaired by suppression of the type 2 signaling and are reversed by recolonization of the antibiotic-treated, or the germ-free mice with microbes. These results provide

[†]Correspondence: Mirko Trajkovski, Mirko.Trajkovski@unige.ch.

Author Contributions

N.S.-Z. and S.F. designed and performed experiments, analyzed data and prepared figures; C.C., O.S., C.V.-D. and A.S. performed experiments and analyzed data; D.J.C., S.G., X.M., and Y.S. did the PET-CT and the CT experiments; V.T. and D.R. participated in experiments and D.R. gave technical support; S.H. and M.I. provided germ-free mice and antibiotics, respectively, and advised on their use; M.T. designed the work, participated in experiments, analyzed data, prepared the figures and wrote the manuscript with input from all co-authors.

Competing financial interests

The authors declare no competing financial interests.

Europe PMC Funders Author Manuscripts

insight into microbiota-fat signaling axis and beige fat development in health and metabolic disease.

The intestinal microbiota is established with the development of the host, and its composition is influenced by several physiological changes, including obesity and pregnancy[5,6,7]. The intestinal microbiota can also influence host metabolism[8] and insulin sensitivity[9,10]. To address the metabolic effects of complete microbiota depletion, we used an antibiotic cocktail supplemented in drinking water (Abx) and germ-free (GF) mice, and in agreement with the previous work[10-12] showed improvements in insulin sensitivity and tolerance to oral and intraperitoneal glucose challenge in both animal models (Fig. 1a–d, Supplementary Fig. 1a–d). The insulin sensitivity of the microbiota-depleted Abx mice was further investigated using hyperinsulinemic-euglycemic clamp in awake and unrestrained C57Bl/6J mice. Antibiotic administration led to a marked increase in the glucose infusion rates needed to maintain the clamped glucose levels, and to an increase in the stimulated rate of whole-body glucose disappearance (Rd) levels, while both the basal, and the final insulin levels were lower (Fig. 1e, Supplementary Fig. 2a,b). These results demonstrate that microbiota depletion improves insulin sensitivity.

To investigate peripheral glucose uptake, we co-administered 2-[^{14}C]deoxyglucose (2[^{14}C]-DG) during the clamp. While no changes were observed in glucose uptake from the interscapular BAT (iBAT), quadriceps muscle, brain, or in hepatic glucose production, there was an increased uptake from the ingSAT and pgVAT, and a decrease from the soleus muscle (Fig. 1f,g, Supplementary Fig. 2c–h). These results suggest that the white fat depots are the main glucose disposal tissues in hyperinsulinemic conditions, which was further corroborated using positron emission tomography-computed tomography (MicroPET-CT). Specifically, [^{18}F]fluorodeoxyglucose ([^{18}F]FDG) uptake in iBAT increased following 12 h cold exposure, but did not differ between the groups. In contrast, Abx mice showed increased [^{18}F]FDG uptake in both ingSAT and pgVAT, which was not changed by cold exposure (Fig. 1h, Supplementary Fig. 3a–d). 2-[1-^{3}H]deoxyglucose (2-DG) uptake during intraperitoneal glucose challenge following 12 h cold exposure further demonstrated that ingSAT and pgVAT are the main glucose disposal tissues affected by microbiota depletion (Supplementary Fig. 3e–j). Together, this demonstrates that microbiota depletion leads to increased glucose disposal specifically in the WAT depots, both in hyperinsulinemic and in basal conditions. Antibiotic treatment also led to a decrease in the volume and weight of ingSAT, pgVAT, and interscapular SAT (iSAT) (Fig. 1i, Supplementary Fig. 4a,b), increased food intake and stool output (Supplementary Fig. 4c–e). These results were consistent with the data we obtained from GF mice, and were confirmed using multidetector computed tomography (CT) (Supplementary Fig. 4f,g). Hounsfield unit analysis of the MicroPET-CT scans revealed that Abx mice had higher ingSAT and pgVAT density compared to controls, and that these differences were increased following 12 h of cold exposure (Fig. 1j, Supplementary Fig. 3j).

We next investigated whether the higher density and the decreased fat amount are originating from differences in adipocyte volume. Measuring the adipocyte size distribution using high content imaging revealed that Abx and GF mice had an increased number of small and a

Europe PMC Funders Author Manuscripts

decreased number of large adipocytes in both ingSAT and pgVAT depots (Fig. 2a,b). Morphologically, there were an increased number of smaller adipocytes in both white fat depots with a multilocular phenotype (Fig. 2c), and the adipose depots excised from the microbiota-depleted animals were darker in appearance (Supplementary Fig. 4h). These features are characteristic of mature beige adipocytes. Therefore, we investigated whether microbiota depletion could affect the browning of the white fat depots. Both Abx and GF mice showed increases in brown fat specific markers in the ingSAT and in the pgVAT depots (Fig. 2d,e). The increased ingSAT and pgVAT browning was confirmed by high content imaging and suggested increased Ucp1-positive cells in both microbiota depleted animal models, accompanied by increased 3,5,3′-Triiodothyronine (T3) levels in the GF mice (Fig. 2f, Supplementary Fig. 5a–c). These data suggest that microbiota depletion leads to browning of white adipose tissues from subcutaneous and visceral depots. The browning was present already 10 days after the microbiota depletion, and further increased after 40 and 60 days (Fig. 2d, Supplementary Fig. 5d–g). Body temperature measurements demonstrated that the initially more pronounced temperature drop observed in Abx mice after acute cold exposure normalized to control levels after six weeks of treatment, despite the lower energy harvest from the food (Supplementary Fig. 5h,i)[13]. Accordingly, mice repopulated with microbiota from control mice, which maintained the increased browning markers 10 days after transplantation, had increased glucose levels during cold exposure, and showed complete tolerance to acute cold (Supplementary Fig. 5i–k) suggesting that the newly developed beige fat is functionally active. The increased thermogenic capacity was further confirmed by oxygen consumption rate (OCR) measurements after isoproterenol stimulation, where adipocytes isolated from the Abx mice showed greater response compared to cells from control mice (Figure 2g).

To investigate the reversibility of the browning after microbiota transplantation, we conventionalized GF mice with microbiota from control (GF conventionalized) or with residual microbiota from Abx mice; expansion of the microbiota in the mice colonized with microbiota from Abx mice was suppressed, or not, with continuous antibiotic treatment of the recipient GF mice (GFAbxT, GFAbxTstop, respectively). Compared to GFAbxT, GF conventionalized and GFAbxTstop mice had decreased glucose tolerance and insulin sensitivity, increased white fat weight and cell size, and diminished browning (as assessed by brown fat marker expression) 5 and 7.5 weeks after transplantation (Fig. 2h–j, Supplementary Fig. 5l–o, Supplementary Fig. 6a–d). GFAbxT and GF mice did not show differences in expression of the browning markers and the size of adipocytes, suggesting that the residual microbiota present after the antibiotic treatment did not affect the increased browning observed in the GF mice (Fig. 2j, Supplementary Fig. 6b–d). These results were consistent with the repopulated Abx mice, which showed decreased glucose tolerance, impaired insulin sensitivity and reversal of the browning of white fat depots after 30 days repopulation (Supplementary Fig. 6e–h). We extended these studies to mice kept at thermoneutrality, where the increased browning capacity would be driven by the microbiota depletion alone, excluding the effect of the environmental temperature[14]. Microbiota depletion also led to increased glucose tolerance and insulin sensitivity at thermoneutral conditions, decreased amounts of ingSAT and pgVAT and smaller adipocytes, along with increased browning markers expression, albeit to a lower magnitude compared to mice kept

at RT, which is consistent with the absence of a mild thermal stimulation (Figure 3a-c, Supplementary Fig. 7a–e). Antibiotic treatment led to improvements in the tolerance to glucose, sensitivity to insulin, increased browning and thermogenic capacity in obese, leptin deficient (ob/ob) and high fat diet (HFD) fed mice (Figure 3d–j, Supplementary Fig. 7f–h), demonstrating that microbiota depletion also promotes improved metabolic fitness of obese animals.

To assess the mechanisms of browning, we profiled the cytokine levels in the ingSAT, and found that several type 1 and 2 cytokines were increased in Abx mice (Supplementary Fig. 8). Eosinophils, and the type 2 cytokines IL-4, IL-13, and IL-5 are sufficient to promote beige fat development through alternative activation of M2 macrophages expressing tyrosine hydroxylase (TH)[15-17,18], a rate-limiting enzyme in catecholamine biosynthesis[19]. These were the most significantly up-regulated cytokines following microbiota depletion in the ingSAT (Fig. 4a), but not in the intestine of the same animals (Supplementary Fig. 8). *Th* mRNA and TH protein levels were increased in ingSAT after 10 d, and still present after 40 and 60 d of microbiota depletion (Fig. 4b–d). The type 2 cytokines were also increased in the pgVAT, but only mildly in the iBAT, bordering significance (Supplementary Fig. 9a,b). Using flow cytometry we detected increased frequency of eosinophils and macrophages in the ingSAT, but not in iBAT of the microbiota-depleted mice. This was accompanied with an enhanced presence of CD301 and TH positive M2-polarized macrophages in the ingSAT (Fig. 4e–g, Supplementary Fig. 9c–k), suggesting that alternatively activated macrophages are associated with the increased ingSAT browning. Accordingly, when compared to the microbiota depleted wt mice, antibiotic-treated IL4 receptor alpha knock-out (*Il4ra*-KO, $Il4ra^{-/-}$) mice showed suppressed cold and glucose tolerance, decreased insulin sensitivity, glucose uptake and browning of ingSAT, but not of pgVAT (Fig. 4h,i, Supplementary Fig. 10a–i). The loss of metabolic improvements in *Il4ra*-KO mice suggests that the ingSAT dominantly contributes to the observed metabolic effects of microbiota depletion, and indicates that additional mechanisms could mediate the pgVAT browning[20]. Finally, increased eosinophil and TH positive M2 macrophages were also detected in ingSAT, but not in pgVAT of the thermoneutral mice after microbiota depletion (Fig. 4j, Supplementary Fig. 10j–l), demonstrating that the increased ingSAT browning and glucose phenotype after the microbiota depletion are mediated by the increased type 2 signaling in both room temperature and thermoneutral mice.

Together, our results demonstrate that microbiota depletion stimulates beige fat development in ingSAT and pgVAT, concomitant with increased type 2 cytokine signaling in these tissues. Inhibition of the type 2 signaling impairs antibiotic-induced subcutaneous fat browning and suppresses the glucose phenotype of the microbiota-depleted mice. This alternative beige fat and macrophage activation opens new insights into the microbiota-fat signaling axis, beige fat development and insulin sensitivity, and suggests novel therapeutic approaches for treatment of obesity and the associated metabolic disorders.

Online Methods

Animals

All C57Bl/6J (wild-type (wt)), BALB/c and *Il4ra*$^{-/-}$ mice were purchased from Charles River, France; ob/ob mice and respective C57Bl/6J controls were acquired from Janvier Labs (France). Mice were kept in a specific pathogen free facility (SPF) in 12 hrs day and night cycles and were fed standard chow or high-fat diet (60% Kcal fat, D12492, Ssniff, Germany). Germ-free (GF) mice were on C57Bl/6 background from the germ-free facility of the University of Bern, and were kept in sterile conditions in 12 hrs day and night cycles until sacrifice, unless otherwise stated. Antibiotics were administered in the drinking water *ad libitum* and replaced with freshly-prepared ones every second day, similar as described previously[21], containing 100μg/ml Neomycin, 50μg/ml Streptomycin, 100U/ml Penicillin, 50μg/ml Vancomycine, 100μg/ml Metronidazole, 1mg/ml Bacitracin, 125μg/ml Ciprofloxacin, 100μg/ml Ceftazidime and 170μg/ml Gentamycin (when longer than 40 days treatment) (Sigma, Germany; Alkaloid, Macedonia). All antibiotic treatments were started at 8 weeks old animals, and all experiments were done in male mice. Cold and thermoneutral exposures were performed at 6°C and 30°C respectively, in a light and humidity controlled climatic chamber (TSE, Germany) in SPF conditions. Acclimatized animals were allocated to groups based on their body weights and blood glucose levels to ensure equal starting points. All mice were kept 2 per cage. All animal experiments were approved by the Swiss federal and Geneva cantonal authorities for animal experimentation (Office vétérinaire federal and Comission cantonale pour les expériences sur les animaux de Genève).

Microbiota repopulation

Abx treated mice were repopulated with microbiota from their conventional former littermates by cohousing for 7 days immediately after antibiotics withdrawal. Mice were analysed at the times indicated in the experiments. For GF repopulation, 500 μl of freshly extracted cecal contents from either conventional or Abx mice were resuspended in 5 ml of anaerobic PBS and 100 μl of the solution was inoculated by oral gavage at days 0 and 2 in each mouse. Animals were kept for 7 days in dirty cages from donor group. Repopulation was confirmed by qPCR.

Hyperinsulinemic euglycemic clamp

Euglycemic hyperinsulinemic clamps were performed in conscious unrestrained catheterized mice at the glucose/insulin clamp platform, University of Geneva. Seven days prior to the experiment, mice were anesthetized using isoflurane and a silastic catheter (0.012 inch inner diameter) was surgically implanted in the right jugular vein and exteriorized above the neck using vascular access button (Instech Laboratories Inc., Plymouth Meeting, PA). Mice were fasted 5 hours before the start of the experiment (t = 0 min). At t = −120 min, an infusion of [1-^{3}H] glucose (0.05 μCi/min) (Perkin Elmer, Walthman, MA, USA) was initiated. After 120 min, blood samples were collected from the tail vein to measure basal blood glucose and plasma insulin as well as to calculate the rate of endogenous glucose appearance (EndoRa) and glucose disposal (Rd) at basal state. At t = 0 min, a continuous insulin infusion (4 mIU/kg body weight/min.) (NovoRapid, Novo Nordisk Pharma, Zurich, Switzerland) was used to induce hyperinsulinemia. The infusion of [3-^{3}H] glucose was increased to 0.1

μCi/min and 50% glucose was infused to maintain target euglycemia (120 mg/dL) (glucose infusion rate, GIR). At steady state, *in vivo* insulin-stimulated glucose uptake in tissues was determined by a 10 μCi bolus injection of 2-[^{14}C] deoxyglucose (2[^{14}C]DG) (Perkin Elmer). After 30 min, mice were killed by cervical dislocation and tissues removed and stored at −80°C until use. [3-^{3}H] glucose and 2[^{14}C]DG specific activities were determined in deproteinized blood samples. Plasma insulin was measured by ELISA (Mercodia, Uppsala, Sweden). EndoRa under insulin stimulated state was determined by subtracting steady state GIR from Rd. Measurements of 2-[^{14}C] deoxyglucose-6-phosphate concentration allowed calculation of the glucose utilization index of individual tissues.

Positron emission tomography - computed tomography (MicroPET-CT)

Mice were anesthetized with 2% isoflurane and were injected in the venous sinus with 5-6 MBq of 2-deoxy-2-[^{18}F]fluoro-*D*-glucose ([^{18}F]FDG). Mice were then left awake at room temperature or at 4°C during the uptake time of 60 min. 10 min prior to positron emission tomography (PET) scan, mice were injected intraperitoneally with 700 μL of 132 mg/mL meglumine ioxitalamate (Telebrix, 6 % m/v iodide, Guerbet AG, Zürich, Switzerland) to delineate the abdominal region and subjected to computed tomography (CT) scans in a Triumph microPET/SPECT/CT system (Trifoil, Chatsworth, CA, USA). Images were obtained at 80 kVp, 160 μA, and 1024 projections were acquired during the 360° rotation with a field of view of 71.3 mm (1.7 × magnification). After 60 min of [^{18}F]FDG uptake, PET scans were started for a total duration of 20 min. PET scans were reconstructed with the built-in LabPET software using an OSEM3D (20 iterations) algorithm and images were calibrated in Bq / mL by scanning a phantom cylinder. The Triumph XO software, which uses a back-projection engine, was used to reconstruct the CT scans with a matrix of 512 and a voxel size of 0.135 mm. CT scans were co-registered with the PET scans using the plugin Vivid (Trifoil) for Amira (FEI, Hillsboro, OR, USA) and exported as dicom files. The software Osirix (Pixmeo, Bernex, Switzerland) was used to quantitatively analyse the datasets and generate pictures. Regions of interest (ROI) were drawn on contiguous slices on CT scans and computed as 3D volumes for the measurements of volumes and densities of indicated adipose tissues. Then, PET series were converted to display Standardised Uptake Values (SUV) adjusted to the body weight of the animals and merged with CT sets. 3D ROIs derived from CT scans were used to quantify the uptake of [^{18}F]FDG in the indicated adipose tissues. In order to measure the volume of activated interscapular BAT, a 3D ROI was first delineated visually by contouring the [^{18}F]FDG activity. A new ROI was then derived based on a threshold equal to the mean [^{18}F]FDG minus one standard deviation of all voxels within the primary defined ROI. This final volume was used to report the activated BAT.

2-[1-^{3}H]deoxyglucose (2DG) uptake

In vivo insulin-stimulated glucose uptake in tissues during the IPGTT was determined by the concomitant injection of 40 μCi of 2DG (Perkin Elmer) with the glucose load (i.p., 2g/kg BW). 2DG specific activity was determined in deproteinized blood samples collected from the tail vein 5, 15, 30 and 45 min after injection. At 45 min, mice were rapidly killed and tissues removed and stored at −80°C until use. Measurements of 2-[1-^{3}H]deoxyglucose-6-

phosphate concentration allowed calculation of the glucose utilization index by individual tissues.

Flow cytometry and characterization of hematopoietic cell populations

Primary stromal vascular fractions (SVF) from ingSAT, pgVAT and iBAT were prepared as described[22,23]. Cells were washed in phosphate-buffered saline (PBS) supplemented with 0.1% BSA and 0.5 mM EDTA, pH 8.0, and stained when appropriate with rat monoclonal anti-F4/80 (Clone A3-1, cat # ab105155, 1:200, Abcam), rat monoclonal anti-CD11b (Clone M1/70, cat # 561114, 1:200, BD Biosciences) and rat monoclonal anti-CD301 (Clone LOM-14, cat # 145705, 1:400, BioLegend) for macrophage staining, or rat monoclonal anti-CD45 (Clone 104, cat #558702, 1:200, BD Biosciences) and rat monoclonal anti-Siglec F (Clone E50-2440, cat # 562068, 1:200, BD Biosciences) for eosinophil staining. For intracellular markers, cells were subsequently washed again, fixed in 2% paraformaldehyde, then labeled with rat monoclonal anti-NOS2 (Clone CXNFT, cat # 61-5920, eBioscience) and rabbit monoclonal anti-TH (Clone EP1533Y, cat # TA303716, 1:50, Origene) and polyclonal goat anti-rabbit secondary antibody (cat # A-10931, 1:400, Thermo Fisher Scientific) in permeabilization buffer (PBS with 0.5% Tween 20). Data were acquired using a Gallios Flow Cytometer (Beckman Coulter) and analyzed with FlowJo v10 software. After gating out dead cells and doublets, macrophages were identified as $CD11b^{+}F4/80^{+}$ and eosinophils were detected as $CD45^{+}Siglec\text{-}F^{+}$ cells.

Calorie uptake

Mice were housed 2 per cage, and food intake and feces production were measured and collected per 24 h. The feces were dried and ground to a fine powder before subjecting them to an oxygen bomb calorimeter (Parr, 6100, USA) according to the manufacturers instructions. Calorie excretion was calculated by multiplying the produced feces with the calories content per gram feces.

Histology, Immunofluorescence and western blotting (WB)

Tissues were extracted, fixed in 4% paraformaldehyde (Sigma), paraffin embedded, cut in 5 μm thick sections and stained with hematoxylin-eosin (H&E) using standard techniques. Immunohistochemistry was done using rabbit anti-UCP1 (Pierce PA1-24894, 1:100) and anti-rabbit Cy3 (Jackson 711165152, 1:250) secondary antibody. Images were acquired using Mirax (Zeiss) and the cell/lipid droplet size quantification was performed using MetaMorph software (V7.7.6.0, Molecular Devices). WB was done on 10-20μg total lysates using rabbit anti-TH (OriGene TA303716, 1:1000), and mouse anti-γ-tubulin (Sigma T6557, 1:5000).

Metabolic experiments

Body temperature was read with infrared camera FLIR E60 (FLIR, UK) from 40cm distance and the data was analyzed by FLIR Tools+ software. We confirmed the consistency with the results by rectal body temperature measurements. Glucose tolerance tests were performed after 6 h fasting by intraperitoneal injection or oral gavage of glucose bolus (2g/kg BW). Insulin tolerance test was performed after a 5 h daytime fast, 0.5U/kg except for HFD-fed

mice (0.75U/kg) and ob/ob mice (2U/kg) (Sigma Aldrich I9278). All mice were sacrificed after 5h fasting. 500µl of blood was taken from terminally anesthetized mice in tubes with 15µl of 0.5 mM EDTA, 4 µl of aprotinin and 4 µl of DPPIV and plasma stored at −80 °C.

Serum T3

Serum concentration of T3 (MyBioSource) was detected following manufacturers instruction.

Oxygen consumption rates (OCR)

Oxygen consumption of isolated mature adipocytes from ingSAT was measured in Clark-type electrode (Rank Brothers Ltd., Cambridge, UK). Mature adipocytes were separated from stromal vascular fraction as previously described[21,22,25] and resuspended in respiration buffer (250 mM sucrose, 50 mM KCl, 20 mM Tris/HCl, 1 mM $MgCl_2$, 5 mM KH_2PO_4 and 20µM EGTA at pH 7.0). Respiration was assessed at basal state, and under β–adrenergic stimulation (10 µM isoproterenol). 20 mM oligomycin, 100 nM carbonyl cyanide-4-phenylhydrazone (FCCP) and 20 µM rotenone were added in 5-15 minutes intervals. Consumption values were normalized to extracted DNA from final mixture. Oxygen consumption was repeated two times for each replicate.

Real Time PCR

One µg of total RNA was used for cDNA preparation with random hexamer primers using High Capacity cDNA Reverse Transcription kit (Applied Biosystems). Steady-state mRNA expression was measured by quantitative real-time PCR using the LightCycler 480 SYBR Green Master I Mix (Roche) with a Mx3005P Real Time PCR System (Stratagene), or 386 well LightCycler 480 II (Roche). Transcript levels were normalized to house keeping beta-2-microglobulin (*B2m*). Primer sequences for real-time PCRs are as previously used[22,23], together with the following for *Th*: 5’-GGTATACGCCACGCTGAAGG-3’ (F) and 5’-TAGCCACAGTACCGTTCCAGA-3’ (R).

Statistics

Unless otherwise specified in the figure legends, significance was calculated using non-paired two tailed Students t test.* $P \leq 0.05$, ** $P \leq 0.01$, *** $P \leq 0.001$, and values show mean ± sd. Sample sizes and animal numbers were chosen based on power calculations of 0.8. All experiments were independently performed at least three times without blinding, and representative values from one experiment are shown. No animals or values were excluded from the analysis.

Supplementary Material

Refer to Web version on PubMed Central for supplementary material.

Acknowledgments

We thank M. Gustafsson Trajkovska, C. Wollheim and R. Coppari for discussions and critical reading of the manuscript; C. Darimont for the help with bomb calorimetric measurements; P. Maechler and M. Karaca for help and discussions with the OCR measurements; S. Startchik for help with image quantifications; [ERC-2013-

StG-281904] to SH for partial funding of the gnotobiotic research; and G. Waksman for support. The research leading to these results has received funding from the European Research Council under the European Union's Seventh Framework Programme (FP/2007-2013) / ERC Grant Agreement n. 336607 [ERC-2013-StG-336607]; the Louis-Jeantet Foundation; Fondation pour Recherches Médicales; Novartis Foundation (14B053) and the Swiss National Science Foundation (SNSF) Professorship (PP00P3_144886) to MT.

References

1. Stanford KI, et al. Brown adipose tissue regulates glucose homeostasis and insulin sensitivity. The Journal of clinical investigation. 2013; 123:215–223. doi:10.1172/JCI62308. [PubMed: 23221344]
2. Wu J, et al. Beige adipocytes are a distinct type of thermogenic fat cell in mouse and human. Cell. 2012; 150:366–376. doi:S0092-8674(12)00595-8 [pii] 10.1016/j.cell.2012.05.016. [PubMed: 22796012]
3. Wu J, Cohen P, Spiegelman BM. Adaptive thermogenesis in adipocytes: Is beige the new brown? Genes Dev. 2013; 27:234–250. doi:27/3/234 [pii] 10.1101/gad.211649.112. [PubMed: 23388824]
4. Peirce V, Carobbio S, Vidal-Puig A. The different shades of fat. Nature. 2014; 510:76–83. doi: 10.1038/nature13477. [PubMed: 24899307]
5. Koren O, et al. Host remodeling of the gut microbiome and metabolic changes during pregnancy. Cell. 2012; 150:470–480. doi:10.1016/j.cell.2012.07.008. [PubMed: 22863002]
6. Ridaura VK, et al. Gut microbiota from twins discordant for obesity modulate metabolism in mice. Science. 2013; 341:1241214. doi:10.1126/science.1241214. [PubMed: 24009397]
7. Liou AP, et al. Conserved shifts in the gut microbiota due to gastric bypass reduce host weight and adiposity. Science translational medicine. 2013; 5:178ra141. doi:10.1126/scitranslmed.3005687. [PubMed: 23536013]
8. Tremaroli V, Backhed F. Functional interactions between the gut microbiota and host metabolism. Nature. 2012; 489:242–249. doi:10.1038/nature11552. [PubMed: 22972297]
9. Cox LM, Blaser MJ. Antibiotics in early life and obesity. Nat Rev Endocrinol. 2015; 11:182–190. doi:10.1038/nrendo.2014.210. [PubMed: 25488483]
10. Chou CJ, Membrez M, Blancher F. Gut decontamination with norfloxacin and ampicillin enhances insulin sensitivity in mice. Nestle Nutr Workshop Ser Pediatr Program. 2008; 62:127–137. discussion 137-140. doi:10.1159/000146256.
11. Backhed F, et al. The gut microbiota as an environmental factor that regulates fat storage. Proceedings of the National Academy of Sciences of the United States of America. 2004; 101:15718–15723. doi:10.1073/pnas.0407076101. [PubMed: 15505215]
12. Hwang I, et al. Alteration of gut microbiota by vancomycin and bacitracin improves insulin resistance via glucagon-like peptide 1 in diet-induced obesity. FASEB J. 2015 doi:10.1096/fj. 14-265983. [PubMed: 25713030]
13. El Kaoutari A, Armougom F, Gordon JI, Raoult D, Henrissat B. The abundance and variety of carbohydrate-active enzymes in the human gut microbiota. Nature reviews. Microbiology. 2013; 11:497–504. doi:10.1038/nrmicro3050.
14. Feldmann HM, Golozoubova V, Cannon B, Nedergaard J. UCP1 ablation induces obesity and abolishes diet-induced thermogenesis in mice exempt from thermal stress by living at thermoneutrality. Cell metabolism. 2009; 9:203–209. doi:10.1016/j.cmet.2008.12.014. [PubMed: 19187776]
15. Ganeshan K, Chawla A. Metabolic regulation of immune responses. Annual review of immunology. 2014; 32:609–634. doi:10.1146/annurev-immunol-032713-120236.
16. Lee MW, et al. Activated type 2 innate lymphoid cells regulate beige fat biogenesis. Cell. 2015; 160:74–87. doi:10.1016/j.cell.2014.12.011. [PubMed: 25543153]
17. Qiu Y, et al. Eosinophils and type 2 cytokine signaling in macrophages orchestrate development of functional beige fat. Cell. 2014; 157:1292–1308. doi:10.1016/j.cell.2014.03.066. [PubMed: 24906148]
18. Martinez FO, Helming L, Gordon S. Alternative activation of macrophages: an immunologic functional perspective. Annual review of immunology. 2009; 27:451–483. doi:10.1146/ annurev.immunol.021908.132532.

19. Nguyen KD, et al. Alternatively activated macrophages produce catecholamines to sustain adaptive thermogenesis. Nature. 2011; 480:104–108. doi:10.1038/nature10653. [PubMed: 22101429]
20. Molofsky AB, et al. Interleukin-33 and Interferon-gamma Counter-Regulate Group 2 Innate Lymphoid Cell Activation during Immune Perturbation. Immunity. 2015 doi:10.1016/j.immuni.2015.05.019. [PubMed: 26092469]

Methods-only references

21. Grivennikov SI, et al. Adenoma-linked barrier defects and microbial products drive IL-23/IL-17-mediated tumour growth. Nature. 2012; 491:254–258. doi:10.1038/nature11465. [PubMed: 23034650]
22. Sun L, Trajkovski M. MiR-27 orchestrates the transcriptional regulation of brown adipogenesis. Metabolism. 2014; 63:272–282. doi:10.1016/j.metabol.2013.10.004. [PubMed: 24238035]
23. Trajkovski M, Ahmed K, Esau CC, Stoffel M. MyomiR-133 regulates brown fat differentiation through Prdm16. Nat Cell Biol. 2012; 14:1330–1335. doi:ncb2612 [pii]10.1038/ncb2612. [PubMed: 23143398]
24. Frezza C, Cipolat S, Scorrano L. Organelle isolation: functional mitochondria from mouse liver, muscle and cultured fibroblasts. Nature protocols. 2007; 2:287–295. doi:10.1038/nprot.2006.478. [PubMed: 17406588]
25. Trajkovski M, et al. MicroRNAs 103 and 107 regulate insulin sensitivity. Nature. 2011; 474:649–653. doi:nature10112 [pii] 10.1038/nature10112. [PubMed: 21654750]

Europe PMC Funders Author Manuscripts

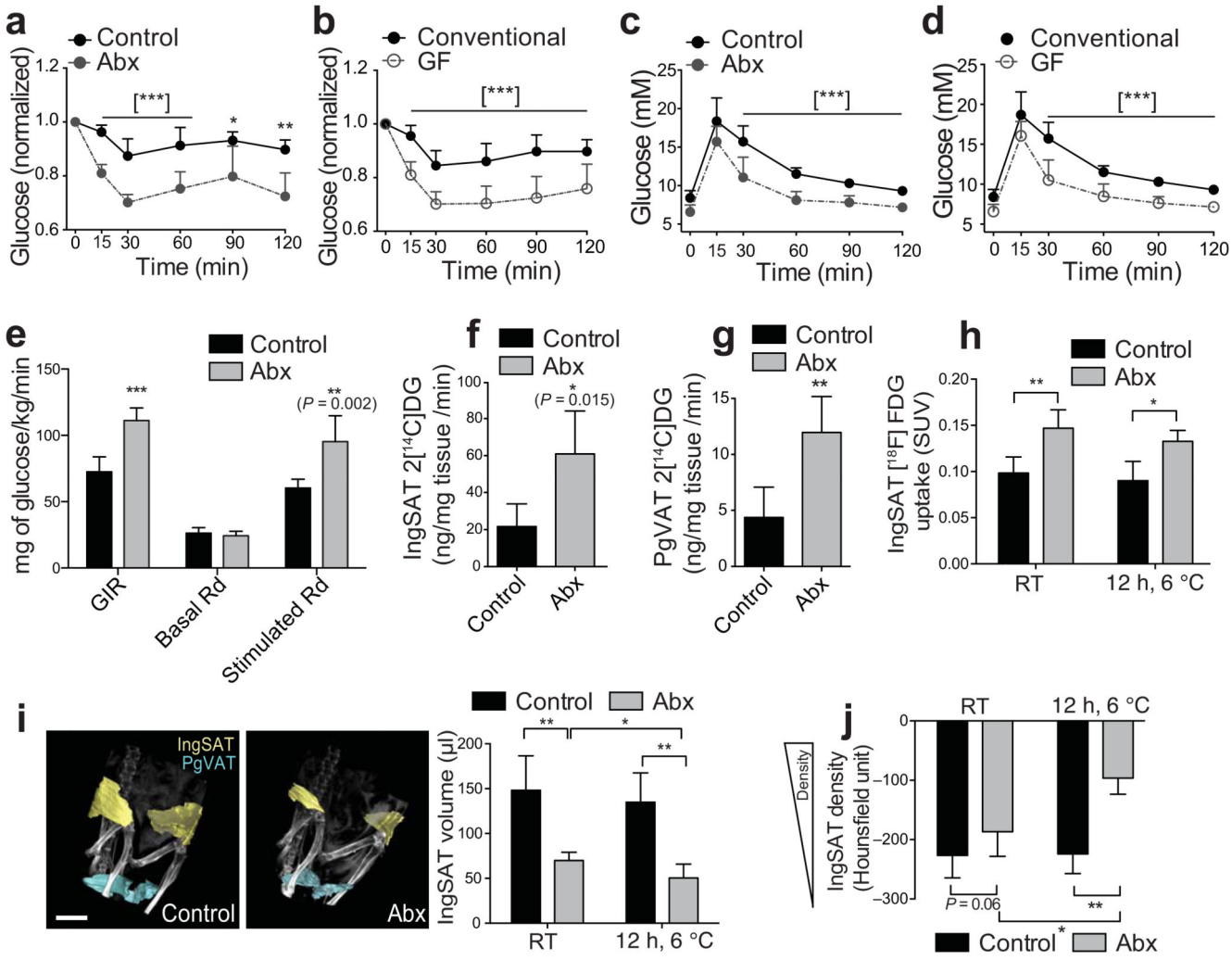

Figure 1.

Microbiota depletion directs glucose uptake primarily to the WAT and improves the sensitivity to insulin. (**a,b**) Insulin tolerance tests (ITT) in Abx (**a**), or GF mice (**b**) compared to the respective controls. Values are normalized to 0 min. (**c**,**d**) Oral glucose tolerance tests (OGTT) of Abx (**c**), or GF mice (**d**) compared to the respective controls. All values in (a-d) show mean ± sd. (n = 8 per group). (**e**) Glucose infusion rate (GIR) and rate of whole-body glucose disappearance (Rd) during hyperinsulinemic-euglycemic clamp in awake and unrestrained C57Bl/6J mice as in (a). Bars show mean ± sd (n = 6 per group). (**f**,**g**) Tissue-specific 2[^{14}C]deoxyglucose (2[^{14}C]-DG) uptake in ingSAT (**f**), and pgVAT (**g**) during hyperinsulinemic-euglycemic clamp in awake C57Bl/6J mice as in (a). (**h**) Standardized Uptake Values (SUVs) of the radiolabeled tracer 2-deoxy-2-[^{18}F]fluoro-D-glucose ([^{18}F]FDG) from the MicroPET-CT in ingSAT in mice as in (a) kept at room temperature, or exposed to 6 °C for 12 hrs. (**i**) 3D reconstitution of the ingSAT and pgVAT (left) and quantification of the total ingSAT volume (right) from mice as in (a) using the MicroPET-CT scans. Scale bar: 5 mm. (**j**) Density of the ingSAT represented in Hounsfield units from mice

Europe PMC Funders Author Manuscripts

as in (a). All bars show mean ± sd (n = 6 per group). Significance was calculated using non-paired two tailed Students t-test.*: $P \leq 0.05$, **: $P \leq 0.01$, ***: $P \leq 0.001$.

Europe PMC Funders Author Manuscripts

Europe PMC Funders Author Manuscripts

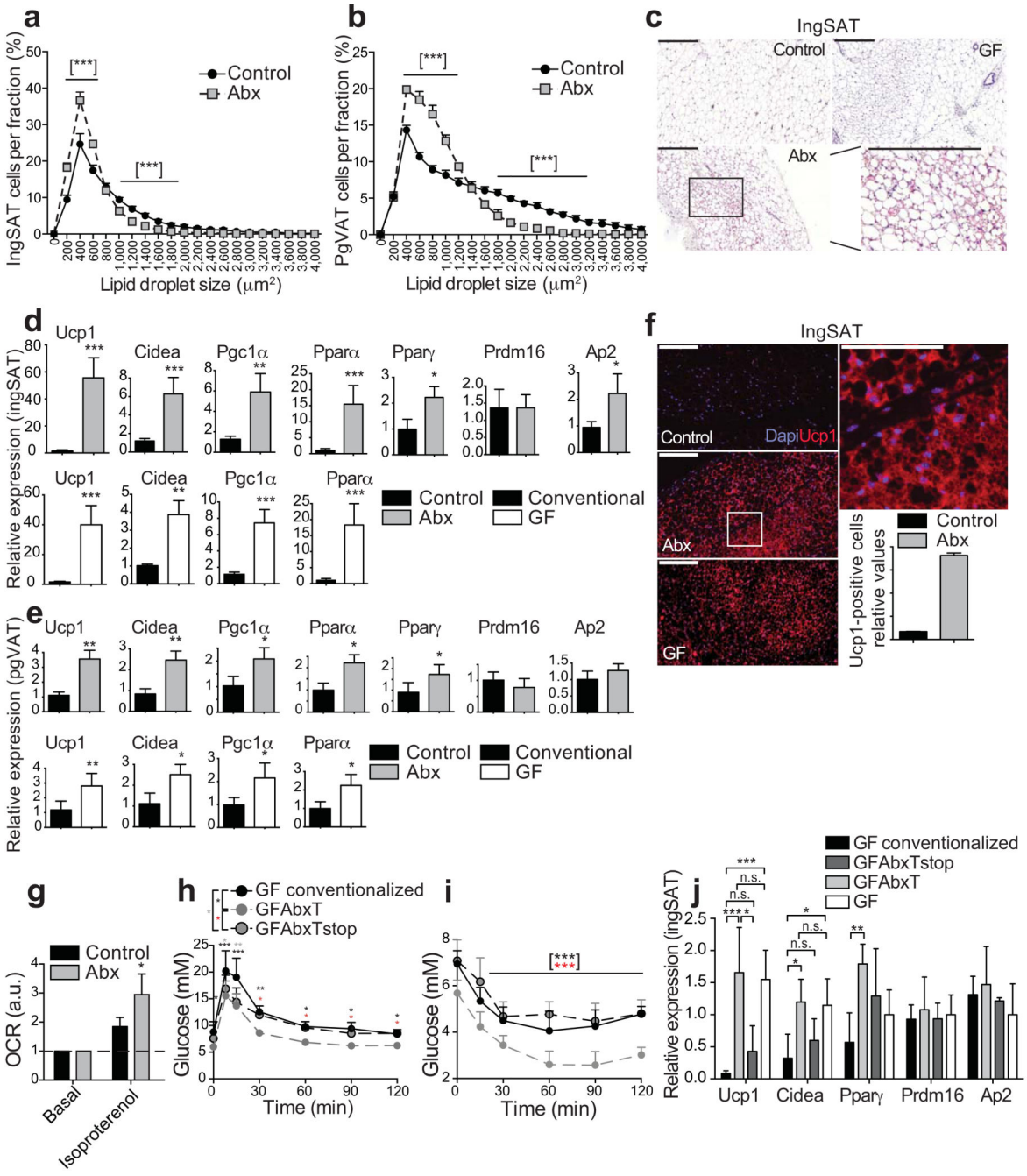

Figure 2.

Microbiota depletion promotes browning of ingSAT and pgVAT. (**a**,**b**) Cell size profiling of adipocytes from ingSAT (**a**) and pgVAT (**b**) fat of control and 40 days treated Abx mice. Points show mean of pooled fractions from each animal ± sem. (n = 6 per group). (**c**) H&E staining on sections from ingSAT of mice at 14 weeks of age. Scale bar: 200 μm. (**d, e**) Relative mRNA expression in ingSAT (**d**), or pgVAT (**e**) of mice as in (a), or GF mice with respective controls. (n = 6 per group). (**f**) Immunohistochemistry on sections from ingSAT of mice at 14 weeks of age. Bars show mean ± sem from automated quantifications of Ucp1-

positive cells relative to total cell number. Scale bars: 200 μm (left) or 100 μm (right). (**g**) Oxygen consumption rates (OCR) of primary isolated ingSAT adipocytes from mice as in (a). Bars represent mean ± sd, calculated using averages of two measurements per condition per pooled sample (*n*) of two mice ($n = 4$ samples, 8 mice per group). (**h**) OGTT of GF mice transplanted with microbiota from control or Abx-treated mice 3.5 weeks after transplantation. Please refer to main text for details. (**i**) ITT of mice as in (h). (**j**) Relative mRNA expression in ingSAT of mice as in (h) 4 weeks after transplantation. All values in (d,e,h-j) show mean ± sd ($n = 6$ per group). Significance was calculated using non-paired two-tailed Students T-test.*: $P \leq 0.05$, **: $P \leq 0.01$, ***: $P \leq 0.001$.

Europe PMC Funders Author Manuscripts

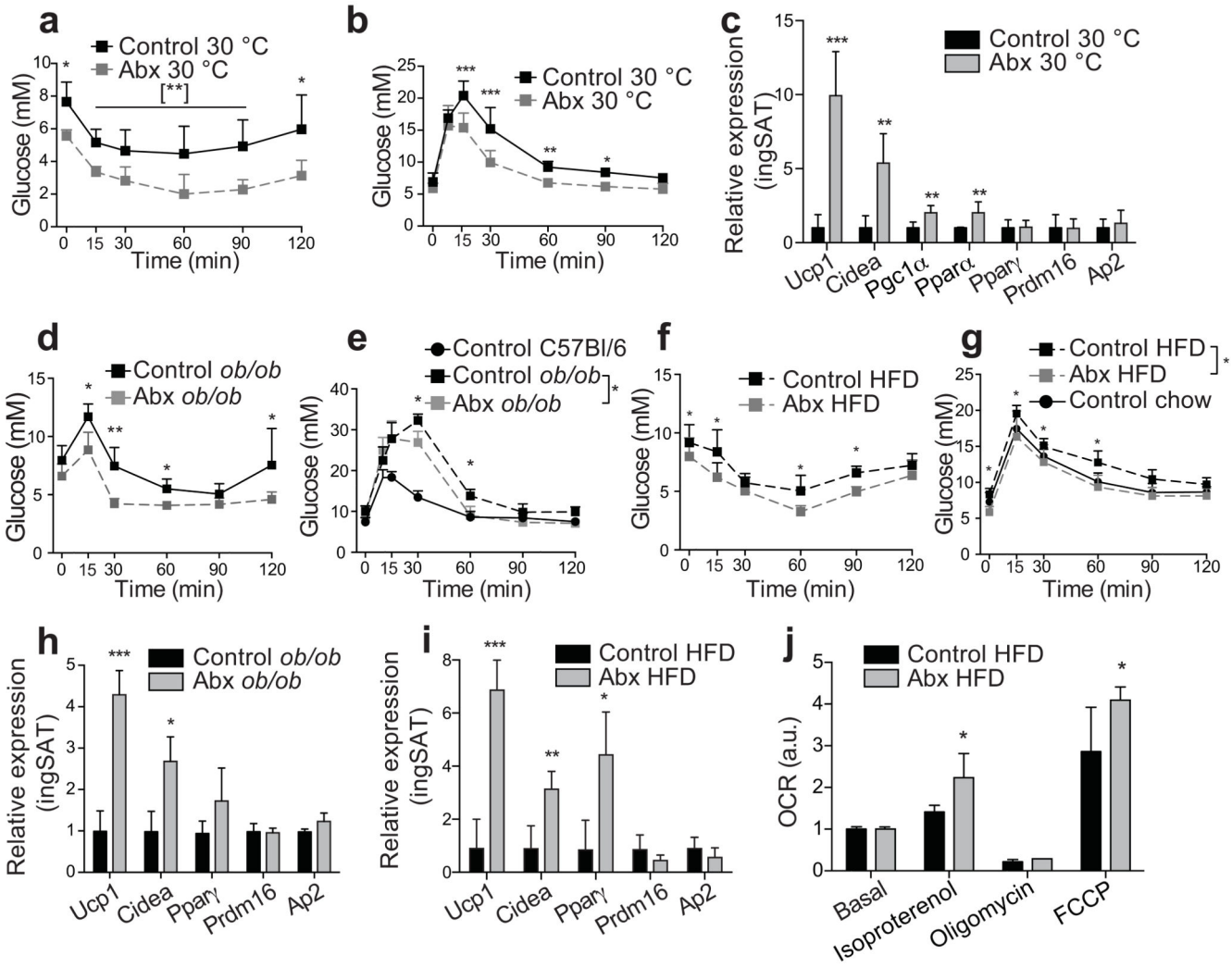

Figure 3.

Microbiota depletion promotes browning in thermoneutral and obese animals and improves metabolic disease. (**a**,**d**,**f**) Insulin tolerance tests (ITT) of wild-type mice in thermoneutral (30 °C) conditions (**a**), of ob/ob (**d**), or HFD (**f**) 40 days treated Abx, or control mice. (**b**,**e**,**g**) Oral glucose tolerance tests (OGTT) of wild-type mice in thermoneutral (30 °C) conditions (**b**), of ob/ob (**e**), or HFD (**g**) 40 days treated Abx, or control mice. (**c**,**h**,**i**) Relative mRNA expression in the ingSAT of wild-type mice in thermoneutral (30 °C) conditions (**c**), ob/ob (**h**), or HFD (**i**) 40 days treated Abx, or control mice, quantified by real-time PCR and normalized to *B2m*. All values in (a-i) show mean ± sd ($n = 6$ for each group). (**j**) Oxygen consumption rates (OCR) of primary isolated ingSAT adipocytes from HFD mice as in f), assessed using Clark electrode and shown after treatment with the indicated drugs used to dissect the multiple components of the cellular respiration, normalized to basal. FCCP: Carbonyl cyanide-*4*-(trifluoromethoxy)phenylhydrazone. Each bar represents mean ± sd, calculated using the averages of two measurements per condition per pooled sample (n) of two mice ($n = 4$ samples, 8 mice per group). Significance was calculated using non-paired two tailed Students T-test. *: $P \leq 0.05$, **: $P \leq 0.01$, ***: $P \leq 0.001$.

Europe PMC Funders Author Manuscripts

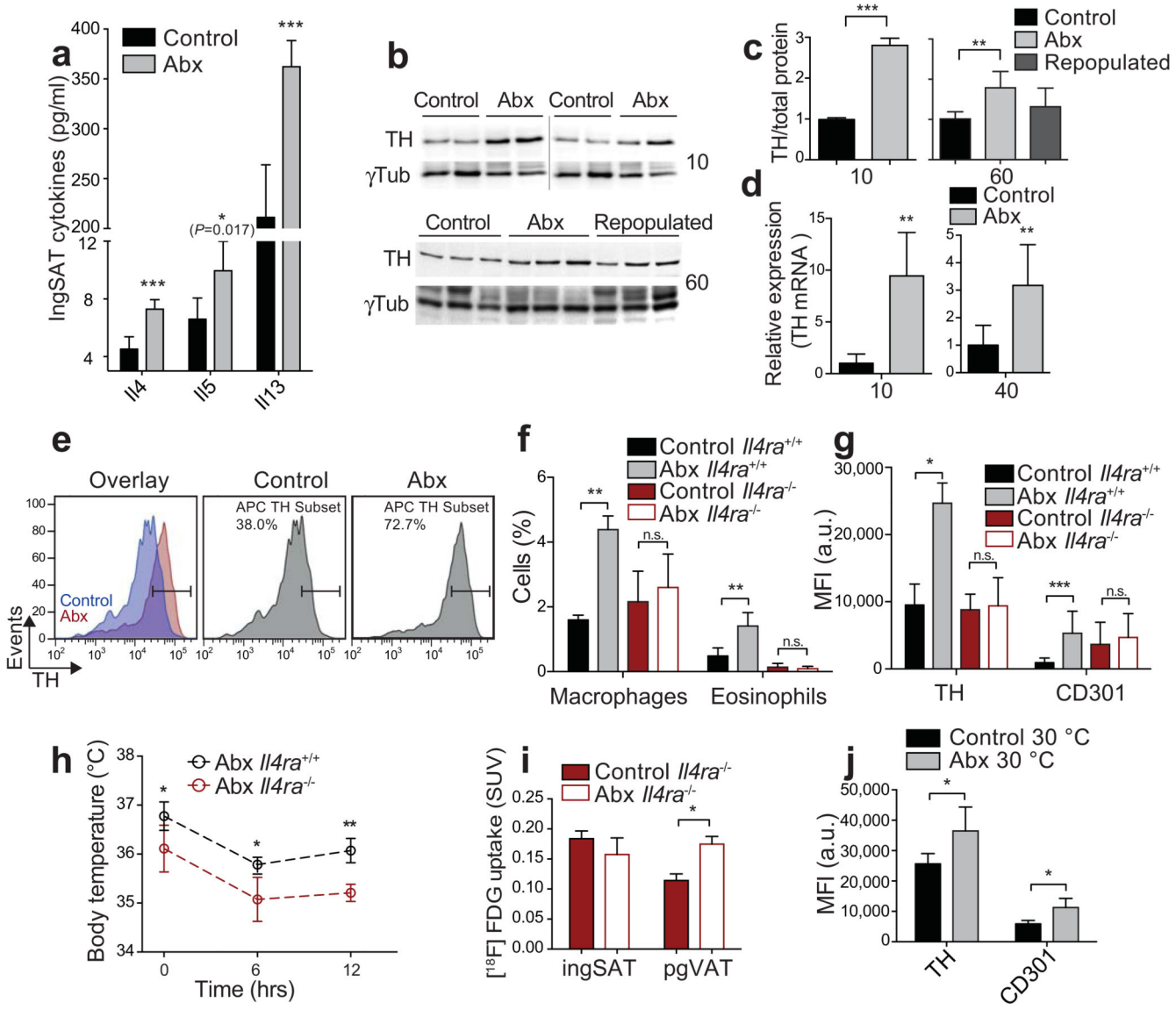

Figure 4.

Browning of ingSAT after microbiota depletion is mediated by type 2 cytokine signaling. (**a**) Cytokine levels in ingSAT of 12 weeks old Abx, or control mice. (n = 6 per group). (**b**,**c**) Western blots (**b**) and quantifications (**c**) of protein lysates from ingSAT of Abx, or control mice after 10, or 60 days antibiotic treatment. (n = 6 per group). γTub: γTubulin. (**d**) Relative *Th* mRNA expression in ingSAT of mice after 10 and 40 days of treatment (n = 6 per group). (**e**) TH expression in F4/80^{+} ingSAT SVF of Abx, or control mice (n = 8 per group). Y axis shows number of events normalized to the mode. (**f**,**g**) Frequency of macrophages and eosinophils (**f**) and Mean Fluorescent Intensity (MFI) of TH or CD301 labeled macrophages (**g**) in ingSAT SVF of control or *Il4ra*$^{-/-}$ mice following antibiotic treatment (n = 4-6 per group). (**h**) Eye body temperature of control or *Il4ra*$^{-/-}$ mice, following antibiotic treatment during cold exposure for 12 h. (**i**) Standardized Uptake Values (SUVs) of the radiolabeled tracer [^{18}F]FDG from the MicroPET-CT in ingSAT and pgVAT

Europe PMC Funders Author Manuscripts

in mice as in (f). (**j**) MFI of TH, or CD301 labeled macrophages in ingSAT tissue of wt mice in thermoneutral (30 °C) conditions treated or not with antibiotics for 40 days ($n = 6$ per group). Values in (a,c,d,f–j) show mean ± sd. Significance was calculated using non-paired two tailed Students T-test. *: $P \leq 0.05$, **: $P \leq 0.01$, ***: $P \leq 0.001$.

Europe PMC Funders Author Manuscripts